ARTICLE

Formation and Instability of Silver Nanofilament in Ag-Based Programmable Metallization Cells

Chang-Po Hsiung,[†,*] Hsin-Wei Liao,[†] Jon-Yiew Gan,[†] Tai-Bo Wu,[†] Jenn-Chang Hwang,[†] Frederick Chen,[‡] and Ming-Jinn Tsai[‡]

[†]Department of Materials Science and Engineering, National Tsing Hua University, Hsinchu, Taiwan 30013, Republic of China, and [‡]Electronics and Optoelectronics Research Laboratory, Industrial Technology Research Institute, Hsinchu, Taiwan 310, Republic of China

ABSTRACT In this paper, we report on the formation and rupture of Ag nanofilament on planar Ag/TiO_2/Pt cells using visual observation. During the forming process, the filament tends to stay very thin. Specifically, it is so thin that it breaks up into a chain of nanospheres (according to Rayleigh instability) right after the formation has been completed. Similar mechanical breakup may also impact vertically stacked cells, causing reliability concerns.

KEYWORDS: TiO_2 · electrochemical cell · resistance switching · conductive filament · Rayleigh instability · Auger spectrometry · scanning electron microscopy · transmission electron microscopy

The semiconductor industry has long conducted research toward the development of a nonvolatile memory (NVM) device in order to replace traditional flash memory because it is rapidly approaching miniaturization limits due to its reliability concerns and insufficient charge storage capacity.[1] Among the next generation of NVMs, including charge storage and resistance change memories, an emerging concept known as *resistance switching memory* is thought to be a good candidate for the next generation of NVM and has garnered scientific and commercial interest.[2]

Resistance switching can be achieved *via* the formation and annihilation of a conductive filament formed between device electrodes, resulting in low and high resistive states. The switching process originates from the motion of charged ions that can be driven by the electric field,[3] and these kinds of ionic species are categorized into two types: one is cation migration (*e.g.*, Ag^+ or Cu^+ ions), which are found in some chalcogenides (Ag−Ge−Se, AgS, and CuS, *etc.*),[4−8] oxides (Cu-doped SiO_2, WO_3, ZrO_2, and TiO_2, *etc.*),[9−14] and amorphous Si;[15−19] the other is related to anion migration[20−29] (*e.g.*, oxygen ions found in oxygen-containing compounds such as TiO_2 and $SrTiO_3$, *etc.*). Among them, Ag- or Cu-based conductive bridge random access memory (CBRAM), or so-called programmable metallization cell (PMC) device, is one of the most promising options among the next generation of NVMs due to its fast switching, low power consumption, high scalability, and superior switching endurance.[4] In this device, a conductive Ag or Cu filament is formed or annihilated *via* an electrochemical redox process during the switching operations. When a positive electric bias is applied on an oxidizable anode (*e.g.*, Ag), the anode will be oxidized and will inject Ag^+ ions into the electrolyte. Then, the ions are reduced to form electrodeposits at the inner cathode (*e.g.*, Pt), thus growing a conductive filament toward the anode. Annihilation of a filament can be achieved *via* oxidation of the filament when the electric bias is applied reversely. The conductive filament of the device can be formed in extremely small size (a few nanometers in diameter), thus making device structure highly scalable. However, in this process, there are some issues that have not been discussed in the literature which are crucial for a basic understanding for the switching mechanism. First, an investigation of the shape and dimension of a filament and its determining parameters is crucial, as these may directly impact the device performance, providing a better understanding of the basic operation of the mechanism. Second, understanding the origin of the instability regarding the low resistance state (LRS) of a PMC device is a key to providing solutions regarding drawbacks germane to the poorly retentive digital state.

Herein, a planar feature of the PMC device is developed in order to make the Ag conductive filament visible and more easily

*Address correspondence to d937524@oz.nthu.edu.tw.

Received for review May 14, 2010 and accepted August 10, 2010.

Published online August 13, 2010. 10.1021/nn1010667

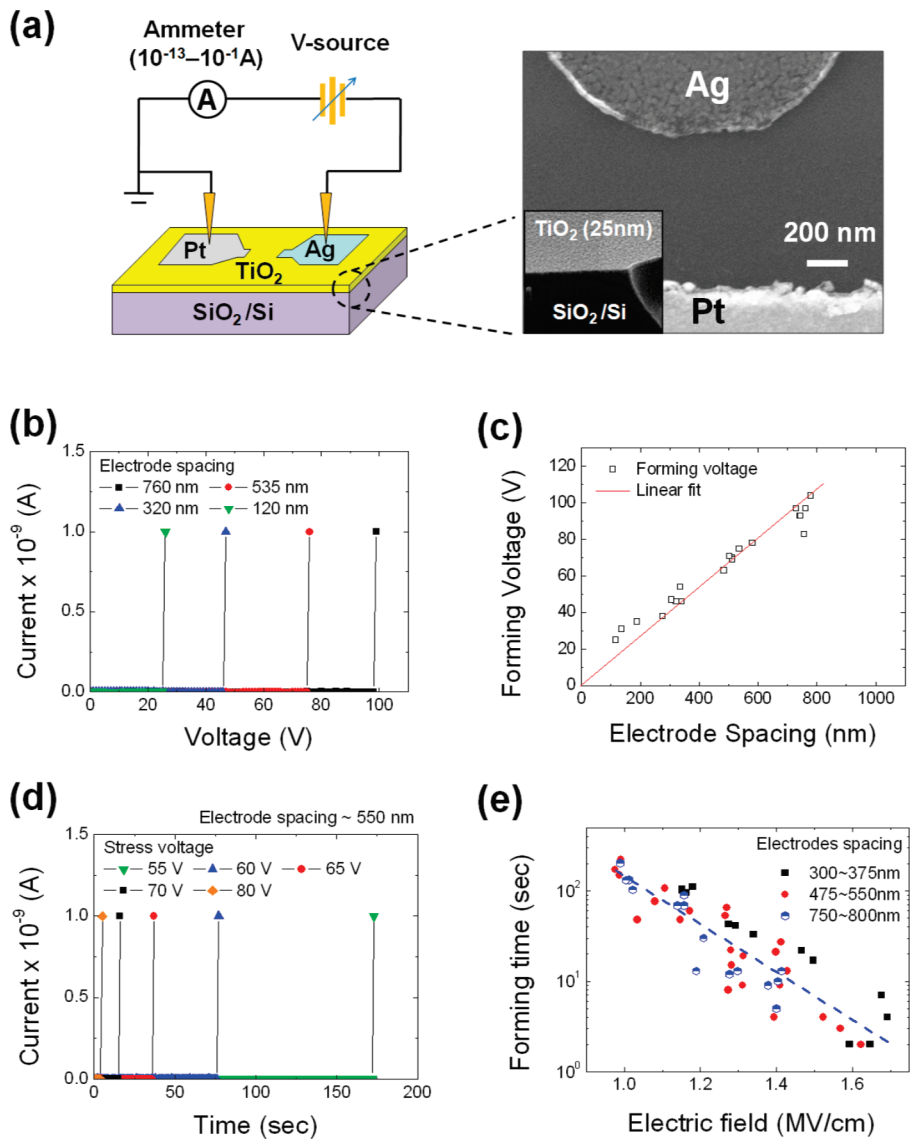

Figure 1. Electrical forming characteristics of a planar Ag/TiO_2/Pt device. (a) Scheme of the planar device. The SEM images shown in the right side are the electrode pads and the 25 nm thick TiO_2 film, showing uniform and flat surface topography. (b) Characteristics of the current *vs* sweeping voltage with various electrode spacings of 120, 320, 535, and 760 nm. (c) Forming voltage as a function of electrodes spacing collected from (b). (d) Characteristics of the current *vs* stressing time under 55, 60, 65, 70, and 80 V. (e) Forming time as a function of stressing electric fields collected from (d).

characterized. A thin Ag nanofilament is formed directly on the electrolytic surface with electrochemical electrodeposition during the forming process. Field-assisted thermally activated hopping of anodic ions (Ag^+) is the responsible mechanism for filament formation and resistive switching. The conductive Ag filament is formed with a cylinder shape and exhibits an ultrasmall dimension, that is, only a few nanometers in diameter. Only one filament is formed during the forming process, and its dimension can be manipulated by controlling the operation current limit. Indeed, such a thin filament is observed to have an impact on the structural instability even at room temperature, as confirmed by the Rayleigh instability proposed in 1878 by Rayleigh, who had initially given the perturbation analysis of one cylinder fluid transformed into a row of spherical droplets due to its unstable nature.[30] Similar mechanical breakup of a thin filament is possible to impact the LRS of vertically stacked cells, causing reliability concerns.

RESULTS AND DISCUSSION

Figure 1a shows the planar device structure used in this work. A TiO_2 electrolyte thin film is coated on the thermally oxidized Si wafers, and the Ag and Pt thin films are used as the coplanar electrodes. The electrical characterization was carried out by applying a positive voltage to the Ag electrode while keeping the Pt counter electrode grounded. Two stressing modes, voltage-sweep and constant-voltage drive, were used to switch the cells on (from a high resistance to a low resistance state). For the former, applied voltage im-

posed on the Ag electrode with a spacing of 120−760 nm from the Pt electrode was swept from 0 V to forming voltage (V_{form}) where current compliance was reached (Figure 1b). The current employed in electroforming, or current compliance (I_{compl}), was restricted to a very low level (≤1 nA) in order to obtain a genuine structure of the formed Ag filament. As the forming voltage is reached, the device resistance is changed from high resistance to low resistance. The decrease of the device resistance indicates that the Ag filament is formed in the device during the electrochemical switching-on process (discussed later). Figure 1c plots V_{form} as a function of the electrode spacing. As shown in the figure, V_{form} is linearly dependent on electrode spacing, indicating that the electric field is responsible for the forming process; the electric field for switching-on is 1.4 MV/cm in the device. In constant-voltage drive, the electrical current was recorded as a function of time while a constant voltage was applied to the Ag electrode. A sharp rise of current is also detected when the electroforming is completed. For the cells with the same electrode spacing, the electroforming process does not seem to be limited by the magnitude of applied voltage, as illustrated in Figure 1d. Instead, it exhibits a longer forming time (t_{form}) using smaller voltage, and *vice versa*. Cells with different electrode spacing were probed with the same constant-voltage drive scheme; the forming time derived from each case was found to fit well with a simple exponential decay function of the apparent electric field (ξ), which is the applied voltage divided with the electrode spacing, as illustrated in Figure 1e. The results show that electroforming is controlled by a field-assisted process instead of a voltage-dependent one.

The same characterization was performed at different temperatures with the cells having the same electrode spacing (300 nm). Each characterizing condition is upon 5 cells on the same chip. As Figure 2a shows, the forming time derived under the same applied voltage is an exponential function of the inverse of temperature (1/*T*), suggesting that electroforming is also a thermally activated process. During forming, two kinds of activation processes should be considered: one is the electrochemical redox reactions at the interface between each electrode and solid electrolyte in which the Butler−Volmer equation is described;[31] the other is the Ag^+ ion migration through the electrolyte. Either of them behaves as an electric field-assisted thermally activated process. In the device, we exclude the electrochemical redox reaction for the following two reasons. First, if the electrochemical reaction is the rate-limited process, it should be true that forming voltage is nonlinearly dependent on the electrodes spacing,[9] which is contradictory to the above finding in Figure 1c. Second, most forming time is expended in Ag^+ hopping across the TiO_2 surface during the forming process, as shown in Supporting Information (Figure S1), indicating

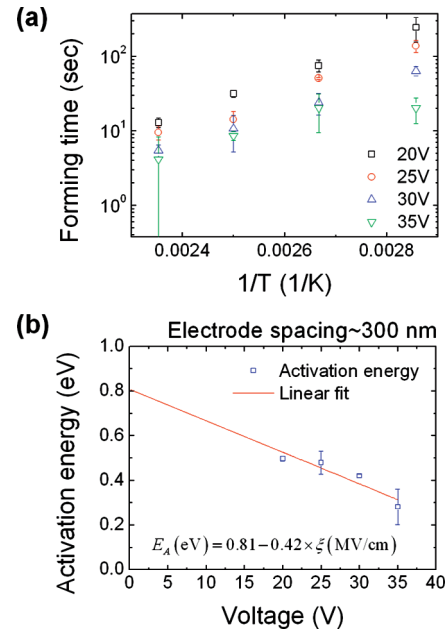

Figure 2. Field-assisted thermally activated hopping of Ag^+ ions on the TiO_2 surface. (a) Forming time as a function of 1/*T* under various dc stressing biases of 20, 25, 30, and 35 V. (b) Activation energy of the Ag filament formation under various stressing biases. The activation energy is calculated by the slopes of forming time *vs* 1/*T* in (a).

that the interfacial electrochemical reaction is not the rate-limited process. Therefore, the dominated activation process of the forming in the device should show Ag^+ ion migration. The activation energy associated with the process can be extracted from the slope in Figure 2a. The activation energy as a function of the applied voltage is plotted in Figure 2b, which shows a linear relation between the activation energy and the apparent electric field: $E_a(\xi) = E_a(0) - qd\xi$, where $E_a(0)$ is 0.81 ± 0.1 eV at the zero electric field and the characteristic length *d* is about 4.2 nm when the apparent electric field is in V/nm. The above results clearly demonstrate that the electroforming of these cells is a field-assisted thermally activated process with the forming speed t_{form}^{-1} proportional to $\exp[-(E_a - qd\xi)/k_BT]$. The same process has also been recognized for the hopping of ionic species in the solids.[32]

The Ag electrodeposits after the forming process were analyzed with scanning electron microscopy (SEM) and high-resolution transmission electron microscopy (HRTEM), as shown in Figure 3. Figure 3a shows the SEM image of the cell after the forming process. The cell is electrically formed under compliance current of 1 nA. It was observed that the Ag electrodeposits were formed between the Ag and Pt electrodes. However, the Ag deposits seem to be composed of a few particles instead of a filament. This may concern how the Ag particles are developed during the forming process; interestingly, the data suggest that the Ag particles are likely formed after the formation of the Ag filament due to the electrical characterization as dis-

cussed below. Figure 3b shows the current−voltage characteristics of the forming process and the subsequent measurement (second switch). The second switch is subsequently performed within 1 s after the forming process. As shown in the figure, the cell remains in a high resistance state even though the cell has been switched on in the forming process. Furthermore, the subsequent measurement shows a smaller switching voltage than that in the forming process (V_{form}) because of the formation of less effective spacing between the electrodes. All of the above support claims that the Ag filament is structurally unstable and tends to break into a number of particles. To investigate the fine structure more informatively, the cross section of the sample is characterized by HRTEM (Figure 3c,d). The sample for characterization is cut by a focused ion beam (FIB) along the filament growth direction. As shown, the Ag particles have a sphere-like shape with uniform dimensions (~8 nm in diameter) and lie on the TiO_2 surface. The enlarged high-resolution and fast-Fourier transform (FFT) images are shown in Figure 3d. The Ag nanospheres are formed with the face-centered cubic crystalline structure of which the indexes of diffraction patterns are identified, showing the pure Ag crystalline structure within the whole sphere. In addition, it is obvious that there is only one filament that is formed during the forming process. In the process, if the Ag electrodeposit is formed at the edge of a cathode in the initial stage, the electric field is more concentrated on the protrusion than any other region of the edge due to less distance from the anode. Consequently, Ag^+ hopping along this protrusion is greatly accelerated (because of field assistance) and leads to formation of only one filament in the whole process.

To investigate the exact mechanism of the structural evolution, a simple model based on thermodynamic theory was constructed to assess whether the process is spontaneous. We assume the Ag spheres with the number of n have evolved from a Ag cylinder (Figure 4a) in which the length and radius of the cylinder are L and r_0, respectively. The aspect ratio (α) is introduced and defined as L/r_0. The average radius of the Ag sphere is r_{sp}. We assume the volume is kept the same during evolution. Thus

$$r_{sp} = \left(\frac{3\alpha}{4n}\right)^{1/3} r_0$$

and the total free energy change, ΔG ($=\Delta G_V + \Delta G_A$), is $2\pi r_0^2 \gamma_A (4.5^{1/3}\alpha^{2/3}n^{1/3} - \alpha - 1)$, where ΔG_V is the volume free energy, ΔG_A is the surface free energy, and γ_A is the specific surface free energy. It is seen that only the change of surface free energy remains in the formula. If the structural evolution is spontaneous, ΔG should be negative. Thus, it follows that $r_0 < r_{sp}/1.5$. Table 1 shows the summary of the parameters calculated from several samples that were tested under the same characterizing conditions (cc = 1 nA). The SEM images of

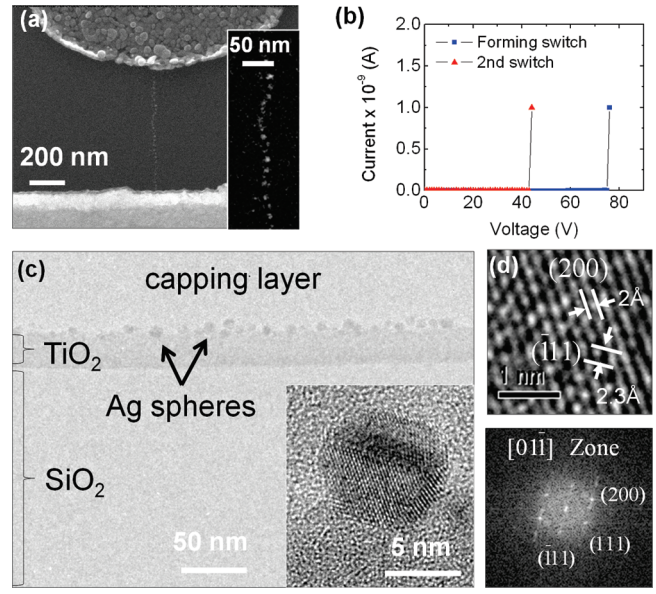

Figure 3. Morphology and structure characterizations of the Ag nanospheres. (a) SEM image of the device after the forming process. (b) Current−voltage characteristics of the forming and subsequent measurements. The set voltage in the second switching is significantly smaller than the prior forming operation due to the reduced effective spacing (L_{eff}) between the two electrodes. (c) Cross-sectional TEM image along the Ag growth direction. The enlarged image of the Ag sphere is shown in the inset. The average dimension of the sphere is ~8 nm in diameter. (d) High-resolution TEM image taken from one of the Ag spheres in (c), showing face-centered cubic single-crystalline structure for which two planes, (200) and (1̄11), are indexed. The bottom image shows the diffraction patterns extracted by the fast Fourier transform.

these samples are shown in Supporting Information (Figure S2). It has been shown that all of the parameters satisfy the criteria, that is, $r_0 < r_{sp}/1.5$ (Figure 4b), indicating that the Ag spheres are formed *via* the structural evolution from the Ag cylinder (filament) by reducing the surface energy (surface tension). A question is

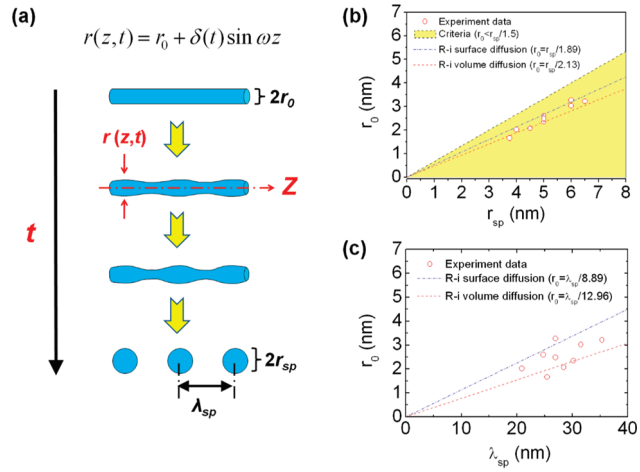

Figure 4. Rayleigh instability (R-i) of the Ag filament. (a) Illustration of the Raleigh instability induced structure evolution of Ag filament. By introducing an infinitesimal longitudinal sinusoidal perturbation in the shape of the cylindrical surface, the equation of the perturbed surface is given by $r = r_0 + \delta \sin \omega z$. (b) Radius of the Ag filament (r_0) as a function of the radius of the Ag sphere (r_{sp}). (c) Radius of the Ag filament (r_0) as a function of the distance between the Ag spheres (λ_{sp}).

TABLE 1. Parameters of the Ag Nanofilament and Nanospheres of the Cells Which Were Tested under the Same Characterizing Conditions (cc = 1 nA)

L (nm)	n	r_{sp} (nm)	r_0 (nm)	α	λ_{sp} (nm)
512	19	6.0	3.3	157	26.9
495	20	5.0	2.6	191	24.8
512	18	4.5	2.1	248	28.4
536	17	6.0	3.0	177	31.5
502	24	4.0	2.0	249	20.9
513	17	5.0	2.4	218	30.2
530	15	5.0	2.2	244	35.3
539	20	5.0	2.5	217	26.9
534	21	3.8	1.7	321	25.4

raised regarding why a filament would always evolve into a number of spheres instead of only one since this is the minimum of the free energy. This type of structural evolution needs to take the kinetic process into account as we have seen for Rayleigh instability. Rayleigh first gave the perturbation analysis for one cylinder fluid into a row of spherical droplets due to its surface tention.[30] Nichols and Mullins performed an analogous treatment for the kinetic process of atomic diffusion on a solid system.[33] In the solid system, the chemical potential (μ) of a surface atom is the product of surface curvature (K), the atomic volume (Ω), and the specific surface energy (γ). The surface atoms diffuse toward a position that has a lower chemical potential or surface curvature. By introducing an infinitesimal longitudinal sinusoidal perturbation in the shape of the cylindrical surface, the equation of the perturbed surface is given by $r = r_0 + \delta \sin \omega z$, where r_0 is the initial cylinder radius, $\omega = 2\pi/\lambda$ is the frequency, λ is the perturbation wavelength, and z is the position along the longitudinal axis (Figure 4a). The surface has two principal curvatures that should be considered: one curvature is the inverse of the radius of a cross section (K_1), and the other curvature is in the cross section of the cylinder along the axial direction (K_2); the two principal curvatures have opposite trends. The curvature K_1 tends to diffuse atoms from the trough to the crest, and the curvature K_2 tends to diffuse atoms from the crest to the trough. The fractional growth rates for various frequencies are described as[33]

$$\frac{\partial \delta}{\partial t}\frac{1}{\delta} = B\omega^2\left(\frac{1}{r_0^2} - \omega^2\right)$$

where $B = D_S\gamma\nu\Omega^2/kT$, and ν is the number of diffusing atoms per unit of surface area. According to the formula, the cylinder is unstable if the perturbation wavelength $\lambda > 2\pi r_0$ (*i.e.*, $\omega < 1/r_0$). On the other hand, the cylinder is stable due to insufficient its longitudinal length. For $\lambda = \lambda_m$, the rate at which the perturbation develops reaches a maximum point; $\lambda_m = 8.89r_0$, $9.02r_0$, and $12.96r_0$ (corresponding with $r_{sp} = 1.88r_0$, $1.89r_0$, and $2.13r_0$, respectively) have been derived for surface (interfacial) diffusion, internal volume diffusion, and external volume diffusion as the dominant transport mechanisms, respectively.[33,34] In our results, r_{sp} and λ_{sp} are, respectively, larger than $1.88r_0$ and $8.89r_0$ and smaller than $2.13r_0$ and $12.96r_0$ (Figure 4b,c). We conclude that surface diffusion may be the dominant transport mechanism due to its extremely small structural dimension.[35] In addition to the intrinsic property of the material, it should be mentioned that the cylinder diameter and the temperature strongly impact the perturbation rate of the structure, as well. The unstable perturbations grow exponentially with time, and the breakup time is proportional to r_0^4.[33] A higher temperature is needed for a cylinder with a larger diameter to realize the perturbation within a limited time, which has been evidenced in the literature regarding Au or Cu cylinders with a diameter larger than 25 nm.[34,36] However, within the small structural dimensions of our Ag filament (<7 nm in diameter), structural perturbation can occur even at room temperatures and finish within a very short time (see Supporting Information).

In vertically stacked programmable metallization cells, the poor retention capability of the LRS is a major obstacle for practical application. The stability of the LRS is deteriorated by an insufficient operating current and relatively high temperature. In switching operations, it has often been reported that the diameter of the filament is decreased with a reduction in current compliance, causing a higher resistance of the LRS.[4] Similar phenomenon is observed in our planar cells, which show a reduction in the radius of the filament with a decreased operating current (Supporting Information, Figure S3). This indicates that the stability of the LRS is closely related to its resistance level and dimensions of the formed filament. Therefore, it is reasonable to conclude that the poor retention capability of the LRS in programmable metallization cells is closely related to its mechanical instability, caused by an insufficient structural size. In the future, a novel switching device, of very small dimensions, such as an atomic switch,[37,38] is an option for achieving low power, high density, and a high speed memory, and the expected impact on retention capability and operational reliability will be a major challenge. To avoid the drawbacks, choosing a suitable material system with lower surface energy between the conductive filament and the solid electrolyte and/or constructing a novel device that can rigidly confine a thin filament may be among the considered options. Nevertheless, since the constructed conditions of vertical cells are different than planar cells, other effects, such as a charge or a strain, must also be considered[39,40] and studied closely in order to achieve the future goal of a reliable CBRAM.

CONCLUSION

In conclusion, formation of Ag nanofilament has been demonstrated using the Ag electrochemical redox process across the planar Ag/TiO_2/Pt structures. No-

tably, field-assisted thermally activated hopping of Ag^+ ions is found to be the responsible mechanism for filament formation. The dimension of the switching filament should be very thin due to low current and fast switching operation; therefore, the thin switching filament may have an impact on the structural instability which results in a poor retention property, most notably for the low resistance state. It is possible to avoid these drawbacks by choosing a suitable material system with lower surface energy or through the design and construction of a novel device that can rigidly confine a thin filament.

EXPERIMENTAL METHODS

Preparation of the Planar Cells. A flat, smooth TiO_2 thin film 10−25 nm thick was deposited with reactive rf sputtering at room temperature on the thermally oxidized Si wafers (thermal oxide ~200 nm thick). Pt (~90 nm thick) and Ag (~30 nm thick) electrodes were subsequently sputter deposited and patterned using the photolithography (I-line stepper, Canon FPA-3000i5+) and the lift-off process. The cells were designed to have a sharp Ag electrode, which is positioned away from the Pt counter electrode, allowing for various spacing between 100 nm and 1 μm. When device preparation is completed, the device chip is subsequently preserved in a dry, vacuum chamber ($\sim 10^{-3}$ Torr, 4% RH) from pollution of moisture and dust in the atmosphere.

Characterizations. The electrical characterizations were performed in the atmosphere (<20% RH for the planar cells) using a Keithley 236 source measurement unit. The surface characteristic of the device is examined using a field-emission scanning electron microscope (FE-SEM, JEOL-6500F). The crystal structure of the Ag spheres is examined using a high-resolution transmission electron microscope (JEOL JEM-3000F).

Acknowledgment. We thank Dr. K.Y. Wu for Auger spectroscopy analysis. This work was supported by the joint program of the Industrial Technology and Research Institute and National Tsing Hua University (99N2461E1).

Supporting Information Available: Nano-Auger spectroscopy characterization and current compliance effect on Ag electrodeposition (SEM images). This material is available free of charge *via* the Internet at http://pubs.acs.org.

REFERENCES AND NOTES

1. International Technology Roadmap for Semiconductors, 2007 edition; www.itrs.net/Links/2007ITRS/ExecSum2007.pdf.
2. Meijer, G. I. Who Wins the Nonvolatile Memory Race? *Science* **2008**, *319*, 1625–1626.
3. Waser, R.; Aono, M. Nanoionics-Based Resistive Switching Memories. *Nat. Mater.* **2007**, *6*, 833–840.
4. Kozicki, M. N.; Park, M.; Mitkova, M. Nanoscale Memory Elements Based on Solid-State Electrolytes. *IEEE Trans. Nanotechnol.* **2005**, 331–338.
5. Liang, C. H.; Terabe, K.; Hasegawa, T.; Negishi, R.; Tamura, T.; Aono, M. Ionic-Electronic Conductor Nanostructures: Template-Confined Growth and Nonlinear Electrical Transport. *Small* **2005**, *1*, 971–975.
6. Liang, C.; Terabe, K.; Tsuruoka, T.; Osada, M.; Hasegawa, T.; Aono, M. AgI/Ag Heterojunction Nanowires: Facile Electrochemical Synthesis, Photoluminescence, and Enhanced Ionic Conductivity. *Adv. Funct. Mater.* **2007**, *17*, 1466–1472.
7. Sakamoto, T.; Sunamura, H.; Kawaura, H.; Hasegawa, T.; Nakayama, T.; Aono, M. Nanometer-Scale Switches Using Copper Sulfide. *Appl. Phys. Lett.* **2003**, *82*, 3032–3034.
8. Sakamoto, T.; Lister, K.; Banno, N.; Hasegawa, T.; Terabe, K.; Aono, M. Electronic Transport in Ta_2O_5 Resistive Switch. *Appl. Phys. Lett.* **2007**, *91*, 092110.
9. Schindler, C.; Staikov, G.; Waser, R. Electrode Kinetics of Cu-SiO_2-Based Resistive Switching Cells: Overcoming the Voltage-Time Dilemma of Electrochemical Metallization Memories. *Appl. Phys. Lett.* **2009**, *94*, 072109.
10. Tsunoda, K.; Fukuzumi, Y.; Jameson, J. R.; Wang, Z.; Griffin, P. B.; Nishi, Y. Bipolar Resistive Switching in Polycrystalline TiO_2 Films. *Appl. Phys. Lett.* **2007**, *90*, 113501.
11. Yang, Y. C.; Pan, F.; Liu, Q.; Liu, M.; Zeng, F. Fully Room-Temperature-Fabricated Nonvolatile Resistive Memory for Ultrafast and High-Density Memory Application. *Nano Lett.* **2009**, *9*, 1636–1643.
12. Kozicki, M. N.; Gopalan, C.; Balakrishnan, M.; Mitkova, M. A Low-Power Nonvolatile Switching Element Based on Copper-Tungsten Oxide Solid Electrolyte. *IEEE Trans. Nanotechnol.* **2006**, *5*, 535–544.
13. Liu, Q.; Dou, C. M.; Wang, Y.; Long, S. B.; Wang, W.; Liu, M.; Zhang, M. H.; Chen, J. N. Formation of Multiple Conductive Filaments in the Cu/ZrO_2:Cu/Pt Device. *Appl. Phys. Lett.* **2009**, *95*, 023501.
14. Yang, L.; Kuegeler, C.; Szot, K.; Ruediger, A.; Waser, R. The Influence of Copper Top Electrodes on the Resistive Switching Effect in TiO_2 Thin Films Studied by Conductive Atomic Force Microscopy. *Appl. Phys. Lett.* **2009**, *95*, 013109.
15. Jafar, M.; Haneman, D. Switching in Amorphous-Silicon Devices. *Phys. Rev. B* **1994**, *49*, 13611–13615.
16. Dong, Y. J.; Yu, G. H.; McAlpine, M. C.; Lu, W.; Lieber, C. M. Si/a-Si Core/Shell Nanowires as Nonvolatile Crossbar Switches. *Nano Lett.* **2008**, *8*, 386–391.
17. Jo, S. H.; Lu, W. CMOS Compatible Nanoscale Nonvolatile Resistance, Switching Memory. *Nano Lett.* **2008**, *8*, 392–397.
18. Jo, S. H.; Kim, K. H.; Lu, W. High-Density Crossbar Arrays Based on a Si Memristive System. *Nano Lett.* **2009**, *9*, 870–874.
19. Jo, S. H.; Kim, K. H.; Lu, W. Programmable Resistance Switching in Nanoscale Two-Terminal Devices. *Nano Lett.* **2009**, *9*, 496–500.
20. Jameson, J. R.; Fukuzumi, Y.; Wang, Z.; Griffin, P.; Tsunoda, K.; Meijer, G. I.; Nishi, Y. Field-Programmable Rectification in Rutile TiO_2 Crystals. *Appl. Phys. Lett.* **2007**, *91*, 112101.
21. Jeong, D. S.; Schroeder, H.; Breuer, U.; Waser, R. Characteristic Electroforming Behavior in Pt/TiO_2/Pt Resistive Switching Cells Depending on Atmosphere. *J. Appl. Phys.* **2008**, *104*, 123716.
22. Yang, J. J.; Pickett, M. D.; Li, X. M.; Ohlberg, D. A. A.; Stewart, D. R.; Williams, R. S. Memristive Switching Mechanism for Metal/Oxide/Metal Nanodevices. *Nat. Nanotechnol.* **2008**, *3*, 429–433.
23. Yang, J. J.; Miao, F.; Pickett, M. D.; Ohlberg, D. A. A.; Stewart, D. R.; Lau, C. N.; Stanley Williams, R. The Mechanism of Electroforming of Metal Oxide Memristive Switches. *Nanotechnology* **2009**, *20*, 215201.
24. Waser, R.; Baiatu, T.; Hardtl, K. H. DC Electrical Degradation of Perovskite-Type Titanates.1. Ceramics. *J. Am. Ceram. Soc.* **1990**, *73*, 1645–1653.
25. Szot, K.; Speier, W.; Carius, R.; Zastrow, U.; Beyer, W. Localized Metallic Conductivity and Self-Healing during Thermal Reduction of $SrTiO_3$. *Phys. Rev. Lett.* **2002**, *88*, 075508.
26. Meijer, G. I.; Staub, U.; Janousch, M.; Johnson, S. L.; Delley, B.; Neisius, T. Valence States of Cr and the Insulator-to-Metal Transition in Cr-Doped $SrTiO_3$. *Phys. Rev. B* **2005**, *72*, 155102.
27. Szot, K.; Speier, W.; Bihlmayer, G.; Waser, R. Switching the Electrical Resistance of Individual Dislocations in Single-Crystalline $SrTiO_3$. *Nat. Mater.* **2006**, *5*, 312–320.

28. Janousch, M.; Meijer, G. I.; Staub, U.; Delley, B.; Karg, S. F.; Andreasson, B. P. Role of Oxygen Vacancies in Cr-Doped $SrTiO_3$ for Resistance-Change Memory. *Adv. Mater.* **2007**, *19*, 2232–2235.
29. Andreasson, B. P.; Janousch, M.; Staub, U.; Meijer, G. I. Spatial Distribution of Oxygen Vacancies in Cr-Doped $SrTiO_3$ during an Electric-Field-Driven Insulator-to-Metal Transition. *Appl. Phys. Lett.* **2009**, *94*, 013513.
30. Rayleigh, L. On the Instability of Jets. *Proc. London Math. Soc.* **1878**, *10*, 4–13.
31. Bockris, J. O. M.; Reddy, A. K. N.; Gamboa-Aldeco, M. *Modern Electrochemistry*; Plenum: New York, 2000.
32. Strukov, D. B.; Williams, R. S. Exponential Ionic Drift: Fast Switching and Low Volatility of Thin-Film Memristors. *Appl. Phys. A* **2009**, *94*, 515–519.
33. Nichols, F. A.; Mullins, W. W. Surface-(Interface-) and Volume-Diffusion Contributions to Morphological Changes Driven by Capillarity. *TMS-AIME* **1965**, *233*, 1840–1848.
34. Karim, S.; Toimil-Molares, M. E.; Balogh, A. G.; Ensinger, W.; Cornelius, T. W.; Khan, E. U.; Neumann, R. Morphological Evolution of Au Nanowires Controlled by Rayleigh Instability. *Nanotechnology* **2006**, *17*, 5954–5959.
35. Gurski, K. F.; McFadden, G. B.; Miksis, M. J. The Effect of Contact Lines on the Rayleigh Instability with Anisotropic Surface Energy. *Siam J. Appl. Math.* **2006**, *66*, 1163–1187.
36. Qin, Y.; Lee, S. M.; Pan, A.; Gosele, U.; Knez, M. Rayleigh-Instability-Induced Metal Nanoparticle Chains Encapsulated in Nanotubes Produced by Atomic Layer Deposition. *Nano Lett.* **2008**, *8*, 114–118.
37. Terabe, K.; Hasegawa, T.; Nakayama, T.; Aono, M. Quantized Conductance Atomic Switch. *Nature* **2005**, *433*, 47–50.
38. Wang, Z. C.; Gu, T. K.; Tada, T.; Watanabe, S. Excess-Silver-Induced Bridge Formation in a Silver Sulfide Atomic Switch. *Appl. Phys. Lett.* **2008**, *93*, 152106.
39. Novo, C.; Mulvaney, P. Charge-Induced Rayleigh Instabilities in Small Gold Rods. *Nano Lett.* **2007**, *7*, 520–524.
40. Qin, Y.; Liu, L. F.; Yang, R. B.; Gosele, U.; Knez, M. General Assembly Method for Linear Metal Nanoparticle Chains Embedded in Nanotubes. *Nano Lett.* **2008**, *8*, 3221–3225.